Thermal–Condensate Collisional Effects on Atomic Josephson Junction Dynamics

atoms

MDPI

Article

Thermal–Condensate Collisional Effects on Atomic Josephson Junction Dynamics

Klejdja Xhani [1,*] and Nick P. Proukakis [2]

[1] Department of Applied Science and Technology (DISAT), Politecnico di Torino, 10129 Torino, Italy
[2] Joint Quantum Centre (JQC) Durham-Newcastle, School of Mathematics, Statistics and Physics, Newcastle University, Newcastle upon Tyne NE1 7RU, UK; nikolaos.proukakis@newcastle.ac.uk
* Correspondence: klejdja.xhani@polito.it

Abstract

We investigate how collisional interactions between the condensate and the thermal cloud influence the distinct dynamical regimes (Josephson plasma, phase-slip-induced dissipative regime, and macroscopic quantum self-trapping) emerging in ultracold atomic Josephson junctions at non-zero subcritical temperatures. Specifically, we discuss how the self-consistent dynamical inclusion of collisional processes facilitating the exchange of particles between the condensate and the thermal cloud impacts both the condensate and the thermal currents, demonstrating that their relative importance depends on the system's dynamical regime. Our study is performed within the full context of the Zaremba–Nikuni–Griffin (ZNG) formalism, which couples a dissipative Gross–Pitaevskii equation for the condensate dynamics to a quantum Boltzmann equation with collisional terms for the thermal cloud. In the Josephson plasma oscillation and vortex-induced dissipative regimes, collisions markedly alter dynamics at intermediate-to-high temperatures, amplifying damping in the condensate imbalance mode and inducing measurable frequency shifts. In the self-trapping regime, collisions destabilize the system even at low temperatures, prompting a transition to Josephson-like dynamics on a temperature-dependent timescale. Our results show the interplay between coherence, dissipation, and thermal effects in a Bose–Einstein condensate at a finite temperature, providing a framework for tailoring Josephson junction dynamics in experimentally accessible regimes.

Keywords: Bose–Einstein condensates; finite temperature; Josephson effect; vortices; collisions; self-trapping

Academic Editor: José Tito Mendonça

Received: 4 June 2025
Revised: 8 July 2025
Accepted: 10 July 2025
Published: 22 July 2025

Citation: Xhani, K.; Proukakis, N.P. Thermal–Condensate Collisional Effects on Atomic Josephson Junction Dynamics. *Atoms* **2025**, *13*, 68. https://doi.org/10.3390/atoms13080068

1. Introduction

A Josephson junction consists of a thin barrier or insulator separating two weakly-coupled superfluids [1–18] or superconductors [19–21]. First studied with superconductors [19–21], it has been shown that a current flows across the junction due to the tunneling of Cooper pairs from one side to the other of the junction. This current could be direct or alternating in the absence or presence of applied external potential, respectively. Josephson effects have been studied extensively, both theoretically and experimentally, with superfluid helium (e.g., [1–4]), trapped ultracold atomic gases [5–18,22–48] (see also [49–56]), and exciton-polariton condensates [57,58]. In particular, one way to induce the Josephson dynamics is by imposing an initial population imbalance between the two superfluids, which induces an initial acceleration of the superfluid across the junction. Previous studies

at $T = 0$ (e.g., [7,15,23,25,37,40]) have revealed the existence of different main dynamical regimes in an atomic Josephson junction: the Josephson plasma, the dissipative, and the self-trapping regime. While individual works had studied transitions between two of those regimes, the three dynamical regimes were first clearly unified into a single Josephson phase diagram in our previous work [38]. The first and the latter regimes are characterized by coherent dynamics, while in the second one, phase slips, well-known from condensed matter systems (see, e.g., [1,59]), lead to the generation of topological defects (the nature of which is set by the underlying system geometry [36–38,60]) and sound waves, with the net effect of inducing dissipation of the Josephson oscillations.

The aim of the present work is to investigate the critical effect that collisions have on these three dynamical regimes when a condensate is coupled to a dynamical thermal cloud. Our study focuses on an elongated three-dimensional geometry, inspired by the experiment of [14,15], where the phase-slip was induced by the generation of vortex rings. In the present work, we will refer to such a dissipative regime as the vortex-induced dissipative regime, in order to distinguish such behavior from the dissipation of the otherwise coherent dynamics arising purely from thermal effects.

To address this, we will use a fully self-consistent model, known as the Zaremba–Nikuni–Griffin, or 'ZNG', model [61–63]: this describes the atomic dynamics in terms of a dissipative Gross–Pitaevskii equation for the condensate, self-consistently coupled to a quantum Boltzmann equation governing the dynamics of the thermal cloud. Such a description includes the full dynamical coupling between the condensate and thermal cloud, e.g., due to their coupled motion, but additionally includes the important effect of collisions, which can either perturb the distribution of particles within the thermal cloud or transfer particles between the condensate and the thermal cloud. Beyond demonstrating the relevance of our studies [37] to experiments and identifying the full Josephson junction dynamical regime phase diagram at $T = 0$ [38], our previous work [39] carefully characterized the effect of the thermal cloud dynamics on the damping and frequency shift of the main oscillation frequencies of the condensate, thermal and total population imbalance within the Josephson plasma, and vortex-induced dissipation regimes. The prior study was conducted within a simplified form of the ZNG model, in which only the self-consistent dynamical coupling of the condensate and thermal cloud was included, but all perturbing collisional effects were ignored. In other words, this corresponded to the Gross–Pitaevskii equation coupled to the collisionless Boltzmann equation. While this should, in principle, be a good approximation at very low temperatures and for relatively short times, collisions are known to affect the overall system dynamics, with their effect increasing with increasing temperatures [64,65].

In the present work, we extend our earlier analysis in two ways: firstly, we revisit the results of [39] in order to investigate the role of such collisional processes on the system dynamics; secondly, we extend such analysis to the Macroscopic Quantum Self-Trapping regime (not previously studied within such formalism), presenting results for both collisionless and collisional implementations of the model. As such, this paper presents a unified view of the role of thermal dissipation across all three distinct Josephson Junction dynamical regimes: Josephson plasma (JP), vortex-induced dissipative (VID), and macroscopic quantum self-trapping (MQST) regimes.

We note that the finite-temperature decay of the self-trapping regime (already experimentally observed in [11]) has also been previously studied in Ref. [34] in the context of an alternative model, known as the stochastic projected Gross–Pitaevskii equation [66]. Rather than making a clear distinction between the condensate and thermal cloud as in ZNG, such a model treats the low-lying modes of the system cumulatively as a classical field while simultaneously ignoring the dynamics of high-lying modes, which are treated as a

reservoir, yielding a dissipative term and a stochastic noise source to the low-lying modes of the system. The relationship between such models has been discussed, e.g., in [63,67–69]. Importantly, for our present work (and leaving aside the comparison of such models), we note that in carrying out their analysis, the work of Ref. [34] fixes the total particle number (up to the imposed energy cutoff) while varying the temperature. Given that the Josephson junction dynamics depend on the condensate number, keeping the total particle number fixed but changing the temperature leads to a different condensate number, which could cause a possible change of the dynamical regime as shown in [39].

Our present study focuses on the effects of the collisions on both the condensate and thermal imbalance dynamics in all three dynamical regimes and for a temperature range $T \leq 0.67T_c$, which is sufficiently far from the critical point. This paper is structured as follows: In Section 2, we describe the numerical methods employed for this study. In Section 3, we show the role of the thermal cloud on different dynamical regimes, while in Section 4, we describe our main conclusions.

2. Methods

We model the system at the finite temperature by numerically solving the *full* Zaremba–Nikuni–Griffin (ZNG) formalism [61–63,67], explicitly including self-consistently obtained collisional terms. This model has been successfully implemented for the study of topological defect dynamics [68,70–73], first and second sound in highly elongated traps [74], evaporative cooling [75], collective modes [64,76–78], and mixtures [65]. It consists of separating the system into two components: the condensate wavefunction $\psi(\mathbf{r}, t)$ and the phase–space distribution function $f(\mathbf{r}, \mathbf{p}, t)$ representing the thermal cloud. As a result, two coupled equations are solved self-consistently; the dissipative Gross–Pitaevskii equation (DGPE) and the Quantum Boltzmann equation (QBE), describing the condensate and thermal cloud dynamics, respectively. The time-dependent DGPE can be written as

$$i\hbar\frac{\partial\psi(\mathbf{r},t)}{\partial t} = \left[-\frac{\hbar^2}{2M}\nabla^2 + V_{\text{ext}}(\mathbf{r}) + g(n_{\text{BEC}}(\mathbf{r},t) + 2n_{\text{th}}(\mathbf{r},t)) - iR(\mathbf{r},t)\right]\psi(\mathbf{r},t) \quad (1)$$

where M is the particle mass (here $^6Li_2$ molecule), V_{ext} the external trapping potential, $g = 4\pi\hbar^2 a/M$ the interaction strength with a the s-wave scattering length between molecules, n_{th} the thermal cloud density, and $n_{\text{BEC}} = |\psi|^2$ the condensate density. The rightmost term within the bracket, $-iR(\mathbf{r}, t)$, represents the dissipative or source (or 'growth'), which facilitates the condensate number to change in time due to the particle exchange with the thermal cloud.

The corresponding equation for the thermal cloud is the Quantum Boltzmann equation for the Wigner phase–space distribution function f in the following form:

$$\frac{\partial f}{\partial t} + \mathbf{v}\cdot\nabla_{\mathbf{r}} f - (\nabla_{\mathbf{r}} V_{\text{eff}}^{\text{th}})\cdot(\nabla_{\mathbf{p}} f) = \mathrm{C}_{12}[f,\psi] + \mathrm{C}_{22}[f] \quad (2)$$

where $V_{\text{eff}}^{\text{th}} = V_{\text{ext}} + 2g(n_{\text{BEC}} + n_{\text{th}})$ is the generalized mean-field potential felt by the thermal particles, and n_{th} is the thermal cloud density obtained through the phase–space distribution f as $n_{\text{th}}(\mathbf{r}, t) = 1/(2\pi\hbar)^3 \int d\mathbf{p}\, f(\mathbf{p}, \mathbf{r}, t)$. Here, the first collisional term includes the collisions between the thermal and condensate particles, which cause particle transfer between the two subsystems, while the second term includes collisions between the thermal particles, which re-distribute the thermal particles between the single-particle states. In the collisional limit considered here, even though the total number is numerically well conserved, the condensate number ($N_{\text{BEC}}(t)$) instead changes in time due to the particle exchange between the condensate and the thermal cloud. This is taken into account in

the C_{12} collisional integral in the Quantum Boltzmann equation; the latter is related to the source term $-iR$ in the dissipative GPE via $R(\mathbf{r},t) = (\hbar/2n_{\rm BEC}) \int d\mathbf{p}/(2\pi\hbar)^3\, C_{12}(\mathbf{p},\mathbf{r},t)$. As a consequence, the thermal cloud particle number, $N_{th}(t)$, also changes in time.

The geometry considered in our study is an anisotropic elongated 3D harmonic trap, with a double-well potential of the following form:

$$\begin{aligned} V_{\rm ext}(x,y,z) &= \frac{1}{2}M\left({\omega_x}^2x^2+{\omega_y}^2y^2+{\omega_z}^2z^2\right) \\ &+ V_0\, e^{-2x^2/w^2}\,. \end{aligned} \tag{3}$$

The values of the trap frequencies are $\omega_x = 2\pi\times 15$ Hz, $\omega_y = 2\pi\times 148$ Hz, and $\omega_z = 2\pi\times 187.5$ Hz along the x, y, and z directions, respectively, chosen to coincide with the experimental values of Ref. [14,15]. The parameters V_0 and w are the Gaussian barrier height and $1/e^2$ width, respectively. Our numerical studies are conducted in a grid of $[-48,48]l_x, [-8,8]l_x, [-8,8]l_x$ along the x, y, and z directions respectively, where $l_x = \sqrt{\hbar/M\omega_x}$, based on $2048\times 128\times 128$ grid points for the thermal cloud. For the less spatially extended condensate, we use a corresponding grid of size $[-24,24]l_x$, with 1024 grid points along the x axis. We initially find the equilibrium state by adding the tilted linear potential $-\epsilon x$ to the $V_{\rm ext}(x,y,z)$. A typical 2D integrated equilibrium profile is shown in Figure 1a for the condensate (i) and the thermal cloud (ii). As evident in this plot, the presence of the repulsive interaction between the condensate and the thermal cloud leads to the thermal particles populating regions of lower condensate density, i.e., at the edges of the condensate or also in the barrier region.

To initiate the dynamics, we instantaneously set the parameter ϵ to zero, thus creating an initial population imbalance, $z_{\rm BEC}(t=0)$, between the two wells. Our earlier work in the limit of a pure $T=0$ condensate revealed that different dynamical regimes emerge depending on the barrier parameters [38]: for relatively small barrier widths or heights, the system transits from the Josephson plasma (JP) to the vortex-induced dissipative regime (VID), with increasing $z_{\rm BEC}(t=0)$, as soon as it exceeds a critical value $z^c_{\rm BEC}$. In the opposite limit of a relatively large barrier height or width the system transits from the Josephson plasma to the macroscopic quantum self-trapping regime (MQST) for $z_{\rm BEC}(t=0)$ beyond the self-trapping critical value $z^{st}_{\rm BEC}$. For our studies here, we fix the Gaussian barrier width at $w = 3.8\xi$, where $\xi = \hbar/\sqrt{2\mu(T=0)M} = 0.52\mu$m denotes the condensate healing length, and change the barrier height. To probe the effect of collisions on these dynamical regimes in the clearest manner, we consider two values for the main barrier height: (i) $V_0 = 104\hbar\omega_x \simeq \mu(T=0)$ for the JP-VID transition and (ii) $V_0 = 210\hbar\omega_x \simeq 2\mu(T=0)$ for the JP-MQST transition. For each dynamical regime, when comparing the results at different temperatures, the barrier height value, V_0 is kept fixed. In order to avoid the possibility of a transition to a different dynamical regime while increasing temperature [found to occur for fixed total number in [39]], all finite-temperature studies presented here are conducted at a fixed *condensate* particle number, $N_{\rm BEC} \simeq 5\times 10^4$. This means that at different temperatures, the total particle number takes different values, increasing with the increasing temperature, in order to keep $N_{\rm BEC}$ fixed.

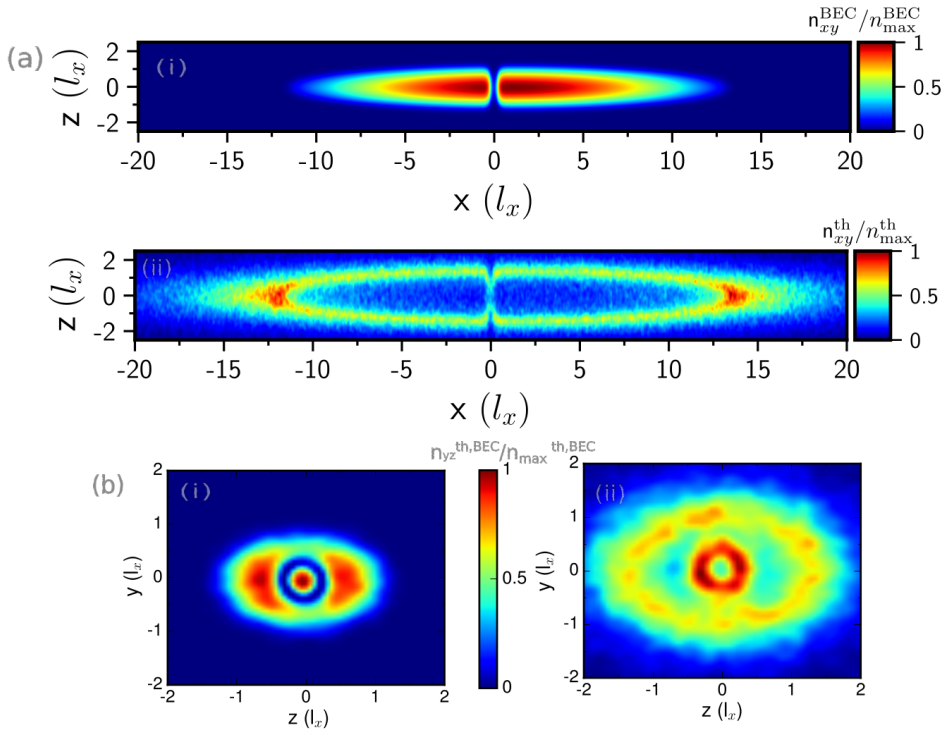

Figure 1. (**a**) Equilibrium 2D integrated condensate (i) and thermal (ii) cloud density in the xz-plane. (**b**) The condensate (i) and thermal density along the yz-plane (ii) extracted at the position of the vortex ring along the x-axis at a fixed time during dynamics. In both cases, the thermal cloud populates the edges of the condensate, and (**b**) (ii) shows that the thermal cloud also populates the vortex core, in addition to the edges of the condensate. The data are obtained at $T = 0.5T_c$ for a fixed condensate number $N_{\rm BEC} \simeq 5.04 \times 10^4$, with a corresponding condensate fraction of $N_{\rm BEC}/N_{\rm tot} \simeq 0.7$, and for barrier height $V_0/\mu(T=0) \simeq 1$ (**a**) and $V_0/\mu(T=0) \simeq 0.6$ (**b**). All densities are scaled to their corresponding maximum values, as indicated by the color bars.

We define the condensate $z_{\rm BEC}(t)$, the thermal cloud $z_{\rm th}(t)$, and the total $z_{\rm tot}(t)$ population imbalances, respectively, as follows:

$$z_{\rm BEC}(t) = \frac{N_{\rm BEC}^R(t) - N_{\rm BEC}^L(t)}{N_{\rm BEC}(t)} \tag{4}$$

$$z_{\rm th}(t) = \frac{N_{\rm th}^R(t) - N_{\rm th}^L(t)}{N_{\rm th}(t)} \tag{5}$$

$$z_{\rm tot}(t) = \frac{N^R(t) - N^L(t)}{N_{\rm tot}} \tag{6}$$

where $N_{\rm BEC}^{\rm R/L}$ and $N_{\rm th}^{R/L}$ are the number of the condensate and thermal particles on the right/left sides of the barrier, respectively, while $N_{\rm BEC}$ and $N_{\rm th}$ are the total thermal and condensate particle number. The presence of a nonzero population imbalance both for the condensate and the thermal particle means that we have a condensate and thermal (or normal) current in the system, with the current extracted as $I = -(N_{\rm BEC/th}/2)(dz_{\rm BEC/th}/dt)$.

While a single numerical run in the absence of collisions generally accurately models the system dynamics, for a systematic monitoring of the results in the collisional case, we generally need to consider a number of (typically five) simulations corresponding to the same physical conditions. Although in the JP and VID regimes, the collisional results are found to exhibit negligible variation from run to run, in the MQST dynamics, the self-trapping decay time is much more sensitive; in the latter case, we thus also perform

multiple MQST runs even for the collisionless regime (in addition to also doing so for the collisional regime).

The condensate imbalance data are analyzed by implementing a two-component fit of the following form:

$$\begin{aligned} F(t) = {} & a_J \cos(2\pi\nu_J t + \phi_J) \exp(-\gamma_J t) \\ & + a_i \cos(2\pi\nu_i t + \phi_i) \exp(-\gamma_i t) \end{aligned} \tag{7}$$

with $a_{J/i}$ and $\nu_{J/i}$ being the amplitude and frequency values of each component, respectively, while $\gamma_{J/i}$ are the damping rates, and $\phi_{J/i}$ the phases of each component. We will show later that the component ν_J, which corresponds to the Josephson plasma, is present in all dynamical regimes. The second component, however, is represented by two different frequencies depending on the temperature and the dynamical regime. These will be denoted as the ν_1 and ν_2 components, i.e., with index $i = 1, 2$ in Equation (7).

3. Results

In this section, we will discuss the role of the thermal cloud dynamics and, in particular, the importance of collisions in each of the three dynamical Josephson junction regimes. This is shown in Figures 2–4 for three different non-zero temperatures, with each figure showing the dynamics of the condensate (left column) and the thermal cloud (right column) without (red lines) and with (black lines) collisions and for each of the three different regimes – from top to bottom showing the Josephson plasma, vortex induced dissipative, and macroscopic quantum self-trapping regimes. For reference, their corresponding $T = 0$ dynamics have been previously discussed at length in Ref. [38].

Specifically, at $T = 0$, the dynamics in the Josephson plasma regime exhibit coherent oscillations about a zero value with constant amplitude in both the condensate population imbalance (or its time derivative, which gives the current) and the Josephson phase (i.e., the phase difference between the two parts of the condensate). Such oscillations persist at relatively low temperatures $T \ll T_c$ (where T_c is the critical temperature), with only very minor damping and collisions having a negligible effect. This can be seen for the specific case of $T = 28\text{nk} = 0.22T_c$ in Figure 2a(i).

In the vortex-induced dissipative (VID) regime, when the dynamics following the initial population imbalance exceeds the local speed of sound, the system is known to generate (potentially successive) vortices, each accompanied by a 2π phase slippage in the relative phase and some sound emission [37]. In the particular geometry, such vortices appear in the form of vortex rings in the transverse plane: such vortex rings can enter and propagate within the bulk condensate and be subsequently observed experimentally, as discussed in [37]. An image of such a vortex ring can be seen in Figure 1b, showing both the condensate density containing the vortex ring (i) and the distribution of the thermal cloud (ii), which is maximized within the low-density region of the vortex ring core and around the condensate. This feature, dominating the dynamics already at $T = 0$ [38], significantly perturbs the subsequent condensate motion, followed by significantly reduced amplitude sinusoidal oscillations of the imbalance around a zero mean value. We observe a similar behavior at $T = 28\text{nK} = 0.22T_c$ of z_{BEC} (t) in both the collisionless and collisional limits [Figure 2b(i)], with collisions having no significant effect.

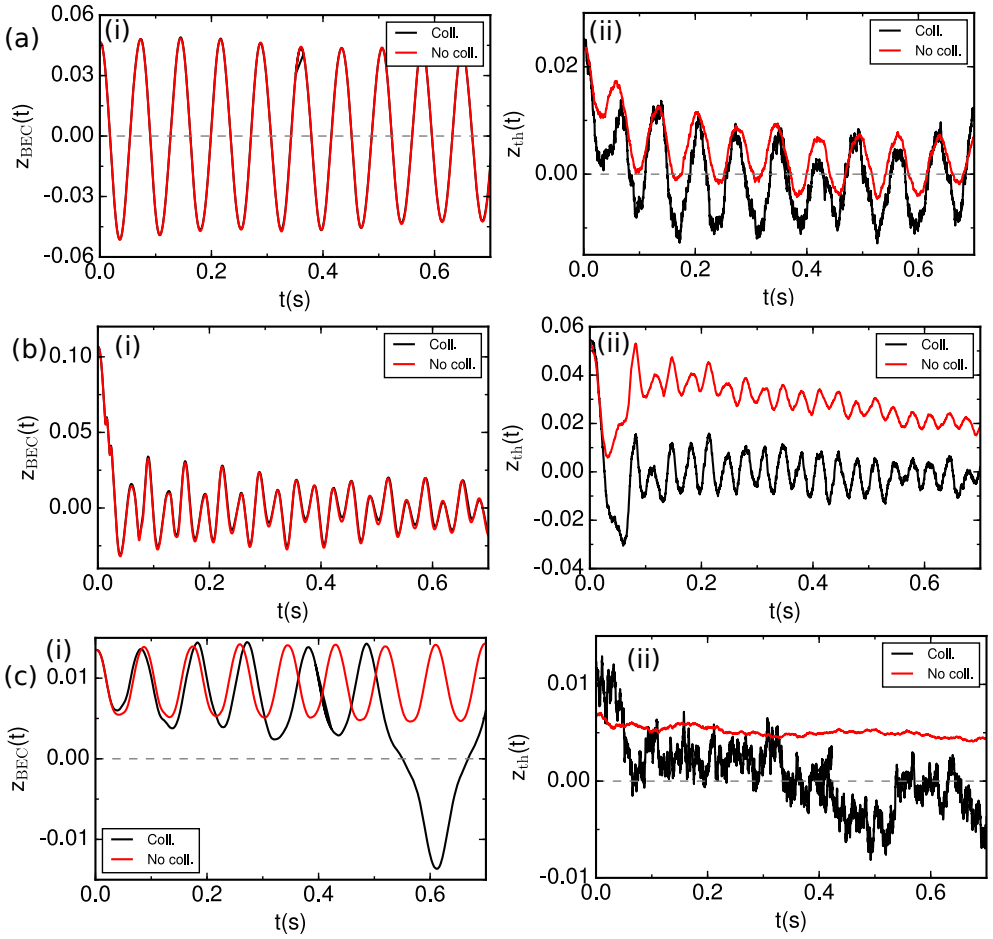

Figure 2. The temporal evolution of the condensate (i) and thermal (ii) population imbalance in the Josephson 'plasma' regime (JP) (**a**), in the vortex-induced dissipative regime (VID) (**b**), and in the macroscopic quantum self-trapping (MQST) regime (**c**) at T =28 nK = $0.22T_c$, both in the collisionless (red line) and collisional limit (black line). The data in (**a**,**b**) are both for barrier height $V_0 \simeq \mu(T=0)$ and initial condensate imbalance $z_{\rm BEC}(t=0) < z^c_{\rm BEC}$ (**a**) and $z_{\rm BEC}(t=0) > z^c_{\rm BEC}$ (**b**), where $z^c_{\rm BEC}$ is the critical imbalance defining the transition from JP to VID regime. The data in (**c**) are for $V_0 = 2\mu(T=0)$ and $z_0 = z^{ST}_{\rm BEC}$, where $z^{ST}_{\rm BEC}$ is the initial population imbalance for which the system transitions from the JP to the MQST regime.

In contrast, the macroscopic quantum self-trapping (MQST) regime at $T = 0$ is characterized by small-amplitude oscillations around a nonzero mean value and 2π phase jumps in the relative phase but without the appearance of propagating vortices and sound waves [38]. In the collisionless limit, the condensate imbalance continues to oscillate around a nonzero mean value at a low temperature, as shown in Figure 2c(i) (red line), with only a very gradual increase in its oscillation amplitude with time. However, when collisions are included, a transition occurs to a different dynamical regime at around $t = 0.5$ s for our specific parameters (see Figure 2c(i), black line); such a regime sees the imbalance oscillate around a zero time-average value, resembling the anharmonic oscillations regime characteristic of the transition to self-trapping [25]. Thus, the inclusion of collisions in the model is in fact essential for accurately describing the self-trapping regime even at low temperatures.

The MQST regime is highly unstable in the presence of a thermal cloud, and its decay time can vary between runs, even in the collisionless limit. Nevertheless, at $T = 0.22T_c$, the imbalance $z_{\rm BEC}$(t) in all five collisionless runs conducted did not decay within the

maximum explored time interval of 0.72 s. In contrast, in the collisional limit, the MQST decayed in all runs, even at this low temperature.

Collisions facilitate thermal equilibration between the two wells across all dynamical regimes, as evidenced in Figure 2a–c(ii). In both Josephson and dissipative regimes—particularly the latter—the thermal imbalance oscillates around a non-zero mean value under collisionless conditions. Collisions suppress this offset, shifting the equilibrium state toward zero thermal imbalance. This contrasts with previous collisionless studies [39], where low-temperature thermal particles relied solely on incoherent tunneling through the barrier. Our results demonstrate that collisional processes, specifically the condensate–thermal particle exchange, enhance such an equilibration. The MQST regime presents unique observational challenges due to its minimal initial thermal imbalance ($z_0^{\mathrm{th}} \simeq 0.01$). This small signal amplitude creates a high noise-to-signal ratio, rendering thermal imbalance oscillations nearly indistinguishable despite their physical presence. The suppression of measurable oscillations persists even when accounting for collisional effects in this regime.

Next, we consider an intermediate temperature $T = 70\mathrm{nK} \approx 0.5\mathrm{T_c}$, selected as the limiting value at which the barrier height practically becomes equal to the temperature, i.e., $V_0 = 104\ \hbar\omega_x \simeq k_B T$. Figure 3 presents the time evolution of both the condensate imbalance z_{BEC} (t) and the thermal imbalance z_{th} (t) across all three regimes at this temperature. In the Josephson (Figure 3a) and dissipative regimes (Figure 3b), the z_{BEC} (t) profiles reveal two key features. First, increasing the temperature leads to stronger damping of the condensate imbalance oscillations, consistent with previous findings [39]. In fact, the presence of a normal current is expected to dampen the Josephson oscillations. Second, collisions further enhance this damping effect, particularly in the dissipative regime, as will be discussed in detail later.

Similarly, collisions significantly reduce the amplitude of z_{th} (t) oscillations compared to the lower temperature case of $T = 0.22T_c$, with the thermal imbalance becoming almost completely damped by $t = 0.4$ s in the dissipative regime (see Figure 3b(ii)). The inset in Figure 3b(i) shows a zoomed-in view of the early-time evolution of z_{BEC}(t), where two distinct 'dips' or 'kinks' appear even in the collisionless limit. These features are signatures of backflow caused by vortex ring generation, as described in [37]. Notably, collisions have little impact on the timing of these dips, which correspond to the vortex ring entering the local Thomas–Fermi surface, and they slightly influence the decay time (i.e., the time when z_{BEC} (t) assumes zero value). At this higher T in the MQST regime, the condensate imbalance decay time and temporal profile differ from run to run, and these differences are even more pronounced in the collisional limit (as will be shown later). Therefore, the particular results shown in Figure 3c represent just one characteristic example among a range of possible behaviors.

Figure 4 instead shows the profiles of z_{BEC} (t) and z_{th}(t) at $T = 0.58T_c$, for which $T > V_0$. We have previously shown [39] that such a condition implies that the thermal cloud can now pass over the barrier, thus being able to execute its own independent oscillations. This new motion can, in turn, significantly affect the condensate dynamics. In the Josephson plasma regime (Figure 4a), collisions cause significantly increased damping of both (i) the condensate imbalance z_{BEC} (t) and (ii) the thermal imbalance z_{th}(t) compared to the collisionless case. Interestingly, in the dissipative regime (Figure 4b), the condensate imbalance starts oscillating with a single dominant frequency, driven by the oscillating thermal component. Thus, in the collisionless limit and in the VID regime, the second component disappears from the condensate imbalance spectrum at a temperature $T_1 = V_0/k_B$. In this regime, collisions have only a minor effect on z_{BEC} (Figure 4b(i)), while they strongly influence the thermal imbalance z_{th}(t) (Figure 4b(ii)). The MQST regime is

included as an example of possible imbalance profiles, but it is important to note that these profiles can vary substantially from run to run.

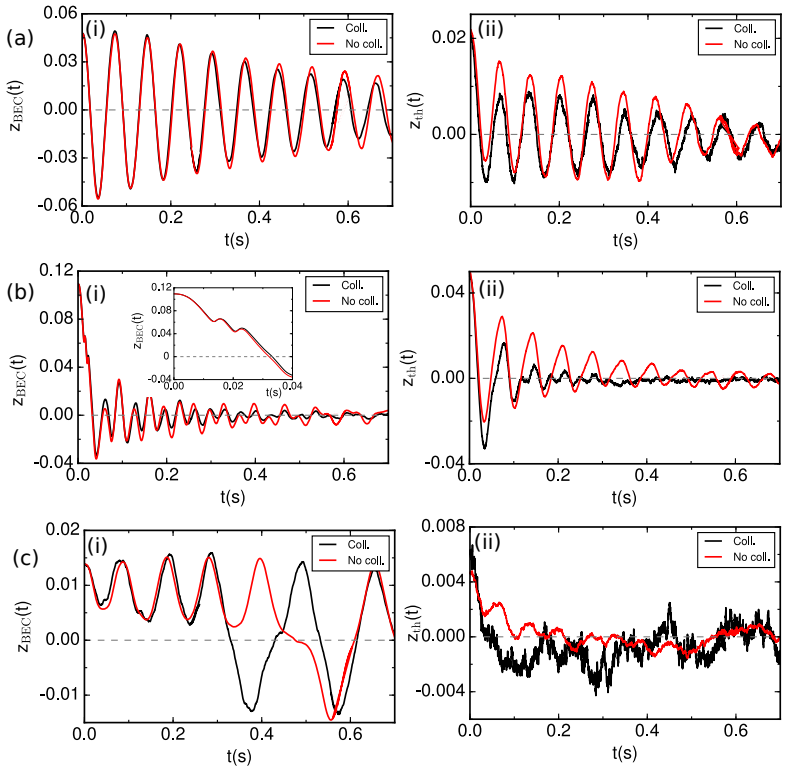

Figure 3. Similarly to Figure 2, but now for $T = 0.5T_c \lesssim V_0/k_B$, marking the highest temperature for which the thermal cloud could not overcome the barrier for the barrier height value in (**a**,**b**). The inset in (**b**) (i) shows a zoomed-in part of the condensate imbalance temporal evolution.

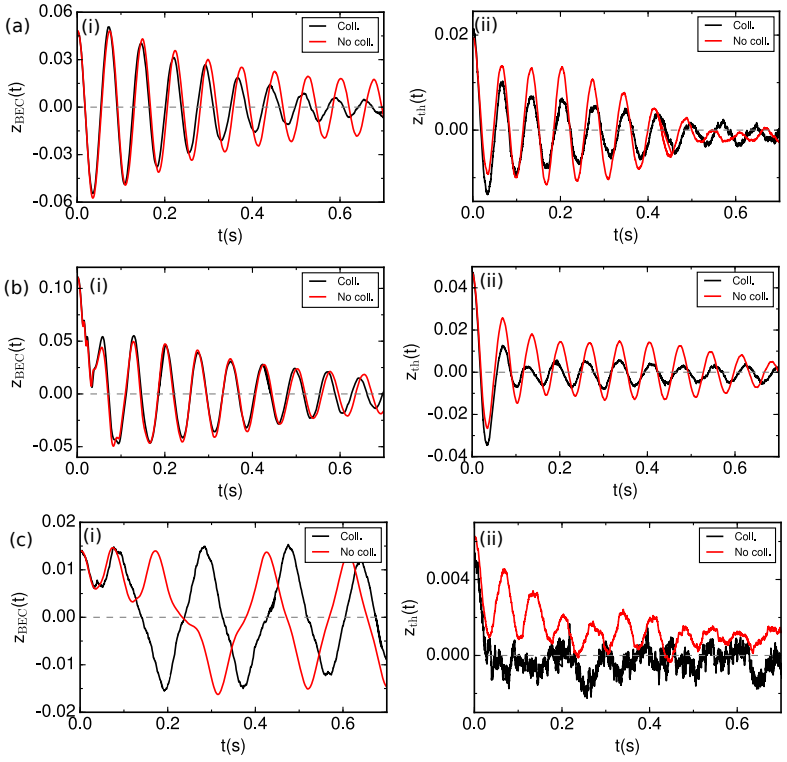

Figure 4. Similarly to Figures 2 and 3, but now for $T = 0.58T_c > V_0/k_B$, such that the thermal cloud can now overcome the barrier on its own for parameters in (**a**,**b**). As such, it suppresses the condensates' sound excitations while also allowing for the thermal cloud to drive the condensate.

3.1. Effect of Collisions on the Frequency and Damping of Dominant Modes in the Josephson Plasma and Vortex-Induced Dissipative Regimes

For both the Josephson and dissipative regimes, we fit the z_{BEC} (t) and z_{tot} (t) at each of the five runs with a two-component frequency fit and take their mean value as the best estimate of our results, with the error bars indicating the maximum deviation.

Consistent with the collisionless results of Ref. [39], the dominant frequencies of both JP and VID at $T \lesssim V_0/k_B \approx 0.5T_c$ correspond to the Josephson plasma frequency ν_J^{BEC} and the frequency $\nu_1^{\mathrm{BEC}} \approx 2\nu_J^{\mathrm{BEC}}$ (attributed to second-order term in the tunneling Hamiltonian). While the Josephson frequency completely dominates the BEC dynamics in the JP regime, the opposite is true in the VID regime, due to the significant sound energy emitted [38]. For $T \approx 0.58T_c > V_0/k_B$, the thermal cloud starts exhibiting its own oscillations over the barrier: such motion emerges in a pronounced way in both dynamical regimes, with the sound waves becoming simultaneously significantly suppressed. In such a limit, we previously found [39] that the system dynamics can once again be described by two dominant frequencies; only now these are the Josephson frequency and a frequency associated with the thermal cloud motion, at a frequency approaching the trap frequency.

It is thus natural to ask how this picture is affected by the presence of collisions: The first observation to make here is that the addition of collisions appears to slightly shift the temperature at which the transition between the low- and high-temperature behaviors emerges to slightly lower values.

The results of the main component frequency value and damping rates as a function of temperature are shown in Figure 5. In particular, Figure 5a shows the dominant frequency value (upper subplots) and damping rates (lower subplots) of the condensate and total imbalance in the Josephson 'plasma' regime. In both cases, the main frequency has a similar value and is close to the expected Josephson plasma frequency; this is why they are called ν_J^{BEC} and ν_J^{tot}. Figure 5b instead shows the corresponding plot for the dissipative regime where now the dominant frequency for $0 < T \leq 0.58T_c$ becomes ν_1^{BEC} for the condensate imbalance and ν_1^{tot} for the total imbalance. In the collisionless limit, the increased temperature shifts towards lower values both the condensate and total imbalance dominant frequency while enhancing their damping due to repulsive interaction with thermal component as in Ref. [39].

In the presence of collisions, two main effects are noted. Firstly, we observe that the inclusion of collisions affects the dominant frequency in the Josephson and dissipative regimes differently both for the condensate and total imbalance. In fact, in the former case, the collisions soften the effect of the decrease in ν_J^{BEC} and ν_J^{tot} with temperature. For $T < 0.5T_c$, the damping rate in the collisional limit has a similar value to the collisionless limit, but when the thermal cloud starts having more of an effect and exhibiting its own motion, i.e. for $T > 0.5Tc = V_0/k_B$, the damping rates γ_J^{BEC} and γ_J^{tot} become larger in the collisional limit. In the dissipative regime instead, the collisions make the ν_1^{BEC}(i) and ν_1^{tot} (ii) achieve smaller values with respect to the collisionless limit (for the same T/T_c) but with a profile similar to the collisionless limit. Moreover, the damping rates γ_1^{BEC} and γ_1^{tot} are larger in the collisional limit in almost the entire range of T.

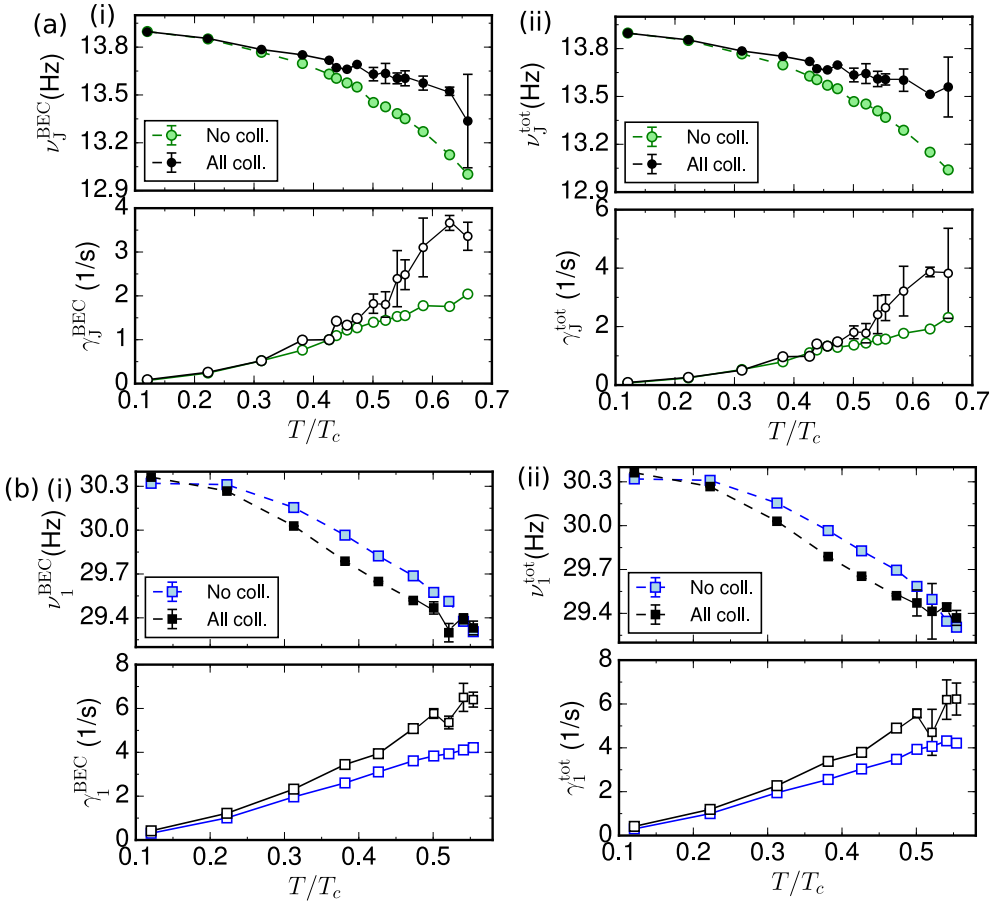

Figure 5. The dominant frequency profile as a function of the temperature and the corresponding damping rates in the Josephson (**a**) and dissipative regimes (**b**) in both the collisionless and collisional limit. In (**a**), the mean values shown in the collisional case are the results from five runs.

3.2. Role of Collisions on the Macroscopic Quantum Self-Trapping

Next, we consider the thermally-induced dissipation of macroscopic quantum self-trapping. The presence of the thermal component induces a normal Ohmic current, i.e., a normal conductance [34] in the system, by causing the dissipation and decay of the condensate imbalance or current oscillations in the self-trapping regime. This decay time can vary significantly from run to run, even in the collisionless limit, as illustrated in Figure 6 for four different temperatures: 28 nK ($0.22T_c$), 62 nK ($0.46T_c$), 70 nK ($0.5T_c$), and 88 nK ($0.58T_c$). At the lowest temperature (28 nK), all runs remain in the self-trapping regime within our probed temporal regime, as shown in Figure 6a. However, as the temperature increases, the influence of the thermal cloud becomes more pronounced, leading to a decay of the self-trapping regime. This behavior is evident at higher temperatures, where the imbalance begins to oscillate around zero, indicating a transition to a different dynamical regime.

To quantify this decay process within our simulated results, we extract the decay time from each run, defined as the time at which the condensate imbalance achieves zero value, and calculate the mean value and associated error bars for both the collisional and collisionless limits, with the results presented in Figure 7. In the collisionless regime, we find that for temperatures below $0.4T_c$, the self-trapping state remains stable throughout the observed time interval (0.72 s), and thus we indicate 0.72s as the lower limit of the expected τ_{MQST} value. As the temperature increases, the self-trapping regime decays progressively earlier, with the decay time decreasing with the temperature. In contrast, in the collisional regime, self-trapping is unstable across the entire temperature range, with a decay time which is shorter than the corresponding time in the collisionless regime. These findings

highlight the significant impact of temperature and interactions on the stability of the self-trapping regime.

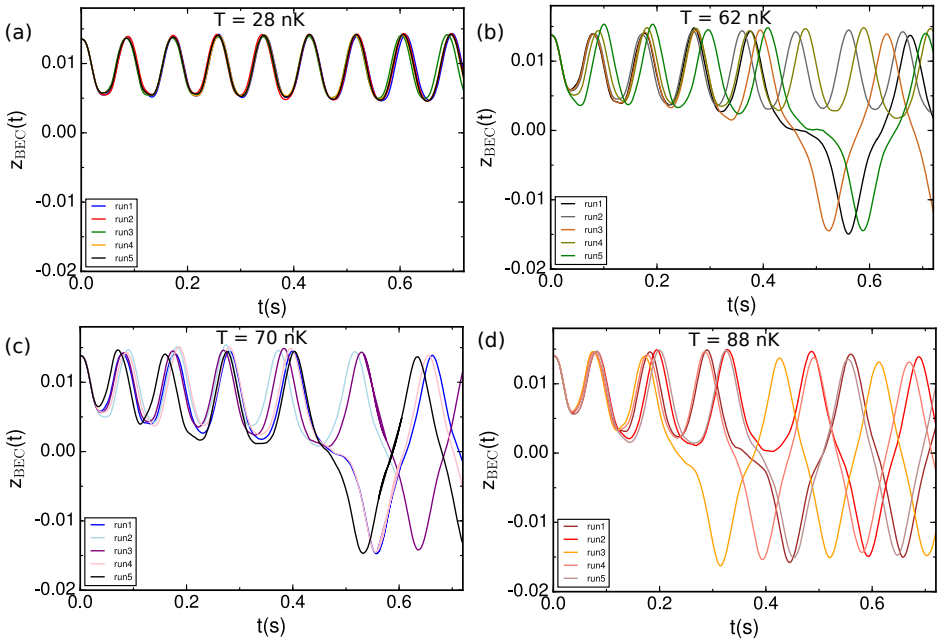

Figure 6. The temporal profile of the condensate imbalance in the collisionless limit at four different temperatures and for five independent numerical runs. The data are for $V_0 = 210\hbar\omega_x$ and $N_{\mathrm{BEC}}(t = 0) = 50{,}400$.

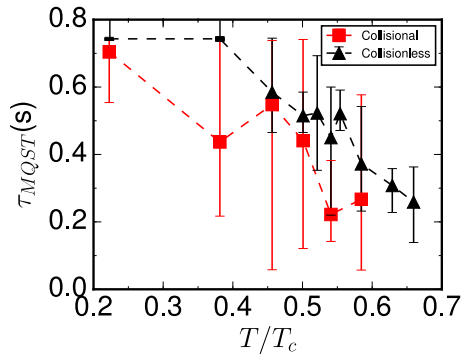

Figure 7. The profile of the mean decay time of the condensate imbalance in the collisionless and collisional limit as a function of the temperature. The data are for $V_0 = 210\hbar\omega_x$ and $N_{\mathrm{BEC}}(t = 0) = 50{,}400$.

4. Conclusions

We investigated the impact of thermal–condensate collisions on the dynamical regimes of a bosonic Josephson junction by numerically solving the full Zaremba–Nikuni–Griffin (ZNG) model, which accounts self-consistently for all collisional processes at finite temperatures. We analyzed how the temperature influences the frequency and damping of the dominant oscillation modes of both the condensate and total current in the Josephson plasma (JP) and vortex-induced dissipative (VID) regimes, as well as the decay time in the macroscopic quantum self-trapping (MQST) regime. Our results show that the decay time in the MQST regime is highly sensitive to collisions even at low temperatures, decreasing as the temperature rises. In contrast, collisions in the JP and VID regimes primarily increase the damping of the condensate modes. Notably, collisions cause a shift toward higher values of oscillation frequency in these regimes. Overall, our study demonstrates that

collisions start playing a crucial role in describing the JP and VID regimes at intermediate to high temperatures, while they are already significant for the MQST regime at low temperatures. It would be interesting to compare our predictions against well-calibrated experimental data in the future.

Author Contributions: Conceptualization of the study K.X. and N.P.P. and numerical simulations and analysis K.X. All authors contributed to the interpretation of the results and to the writing of the manuscript. All authors have read and agreed to the published version of the manuscript.

Funding: This research received no external funding.

Data Availability Statement: Data presented in this paper are available from the corresponding author upon reasonable request.

Conflicts of Interest: The authors declare no conflict of interest. The funders had no role in the design of the study; in the collection, analyses, or interpretation of data; in the writing of the manuscript; or in the decision to publish the results.

Abbreviations

The following abbreviations are used in this manuscript:

BEC	Bose–Einstein condensate
GPE	Gross–Pitaevskii equation
ZNG	Zaremba–Nikuni–Griffin
JP	Josephson Plasma
VID	Vortex-Induced Dissipation
MQST	Macroscopic Quantum Self-Trapping

References

1. Avenel, O.; Varoquaux, E. Josephson effect and quantum phase slippage in superfluids. *Phys. Rev. Lett.* **1988**, *60*, 416–419. [CrossRef] [PubMed]
2. Davis, J.C.; Packard, R.E. Superfluid ^{3}He Josephson weak links. *Rev. Mod. Phys.* **2002**, *74*, 741–773. [CrossRef]
3. Sato, Y.; Hoskinson, E.; Packard, R. Josephson Effects in Superfluid Helium. In *Fundamentals and Frontiers of the Josephson Effect*; Tafuri, F., Ed.; Springer: Cham, Switzerland, 2019; Volume 286.
4. Hoskinson, E.; Sato, Y.; Hahn, I.; Packard, R.E. Transition from phase slips to the Josephson effect in a superfluid 4He weak link. *Nat. Phys.* **2006**, *2*, 23–26. [CrossRef]
5. Anderson, B.P.; Kasevich, M. Macroscopic quantum interference from atomic tunnel arrays. *Science* **1998**, *282*, 1686. [CrossRef]
6. Cataliotti, F.S.; Burger, S.; Fort, C.; Maddaloni, P.; Minardi, F.; Trombettoni, A.; Smerzi, A.; Inguscio, M. Josephson Junction Arrays with Bose-Einstein Condensates. *Science* **2001**, *293*, 843–846. [CrossRef]
7. Albiez, M.; Gati, R.; Fölling, J.; Hunsmann, S.; Cristiani, M.; Oberthaler, M.K. Direct Observation of Tunneling and Nonlinear Self-Trapping in a Single Bosonic Josephson Junction. *Phys. Rev. Lett.* **2005**, *95*, 010402. [CrossRef]
8. Anker, T.; Albiez, M.; Gati, R.; Hunsmann, S.; Eiermann, B.; Trombettoni, A.; Oberthaler, M.K. Nonlinear Self-Trapping of Matter Waves in Periodic Potentials. *Phys. Rev. Lett.* **2005**, *94*, 020403. [CrossRef]
9. Schumm, T.; Hofferberth, S.; Andersson, L.M.; Wildermuth, S.; Groth, S.; Bar-Joseph, I.; Schmiedmayer, J.; Krüger, P. Matter-wave interferometry in a double well on an atom chip. *Nat. Phys.* **2005**, *1*, 57–62. [CrossRef]
10. Shin, Y.; Saba, M.; Pasquini, T.A.; Ketterle, W.; Pritchard, D.E.; Leanhardt, A.E. Atom Interferometry with Bose-Einstein Condensates in a Double-Well Potential. *Phys. Rev. Lett.* **2004**, *92*, 050405. [CrossRef]
11. Levy, S.; Lahoud, E.; Shomroni, I.; Steinhauer, J. The a.c. and d.c. Josephson effects in a Bose–Einstein condensate. *Nature* **2007**, *449*, 579–583. [CrossRef]
12. Spagnolli, G.; Semeghini, G.; Masi, L.; Ferioli, G.; Trenkwalder, A.; Coop, S.; Landini, M.; Pezzè, L.; Modugno, G.; Inguscio, M.; et al. Crossing Over from Attractive to Repulsive Interactions in a Tunneling Bosonic Josephson Junction. *Phys. Rev. Lett.* **2017**, *118*, 230403. [CrossRef]
13. LeBlanc, L.J.; Bardon, A.B.; McKeever, J.; Extavour, M.H.T.; Jervis, D.; Thywissen, J.H.; Piazza, F.; Smerzi, A. Dynamics of a Tunable Superfluid Junction. *Phys. Rev. Lett.* **2011**, *106*, 025302. [CrossRef] [PubMed]
14. Valtolina, G.; Burchianti, A.; Amico, A.; Neri, E.; Xhani, K.; Seman, J.A.; Trombettoni, A.; Smerzi, A.; Zaccanti, M.; Inguscio, M.; et al. Josephson effect in fermionic superfluids across the BEC-BCS crossover. *Science* **2015**, *350*, 1505–1508. [CrossRef] [PubMed]

15. Burchianti, A.; Scazza, F.; Amico, A.; Valtolina, G.; Seman, J.A.; Fort, C.; Zaccanti, M.; Inguscio, M.; Roati, G. Connecting Dissipation and Phase Slips in a Josephson Junction between Fermionic Superfluids. *Phys. Rev. Lett.* **2018**, *120*, 025302. [CrossRef]
16. Kwon, W.J.; Del Pace, G.; Panza, R.; Inguscio, M.; Zwerger, W.; Zaccanti, M.; Scazza, F.; Roati, G. Strongly correlated superfluid order parameters from dc Josephson supercurrents. *Science* **2020**, *369*, 84–88. [CrossRef]
17. Luick, N.; Sobirey, L.; Bohlen, M.; Singh, V.P.; Mathey, L.; Lompe, T.; Moritz, H. An ideal Josephson junction in an ultracold two-dimensional Fermi gas. *Science* **2020**, *369*, 89–91. [CrossRef]
18. Del Pace, G.; Kwon, W.J.; Zaccanti, M.; Roati, G.; Scazza, F. Tunneling Transport of Unitary Fermions across the Superfluid Transition. *Phys. Rev. Lett.* **2021**, *126*, 055301. [CrossRef]
19. Josephson, B.D. Possible new effects in superconductive tunnelling. *Phys. Lett.* **1962**, *1*, 251–253. [CrossRef]
20. Anderson, P.W.; Rowell, J.M. Probable Observation of the Josephson Superconducting Tunneling Effect. *Phys. Rev. Lett.* **1963**, *10*, 230–232. [CrossRef]
21. Barone, A.; Paterno, G. *Physics and Applications of the Josephson Effect*; John Wiley: New York, NY, USA, 1982.
22. Milburn, G.J.; Corney, J.; Wright, E.M.; Walls, D.F. Quantum dynamics of an atomic Bose-Einstein condensate in a double-well potential. *Phys. Rev. A* **1997**, *55*, 4318–4324. [CrossRef]
23. Smerzi, A.; Fantoni, S.; Giovanazzi, S.; Shenoy, S.R. Quantum Coherent Atomic Tunneling between Two Trapped Bose-Einstein Condensates. *Phys. Rev. Lett.* **1997**, *79*, 4950–4953. [CrossRef]
24. Zapata, I.; Sols, F.; Leggett, A.J. Josephson effect between trapped Bose-Einstein condensates. *Phys. Rev. A* **1998**, *57*, R28–R31. [CrossRef]
25. Raghavan, S.; Smerzi, A.; Fantoni, S.; Shenoy, S.R. Coherent oscillations between two weakly coupled Bose-Einstein condensates: Josephson effects, π oscillations, and macroscopic quantum self-trapping. *Phys. Rev. A* **1999**, *59*, 620–633. [CrossRef]
26. Ruostekoski, J.; Walls, D.F. Bose-Einstein condensate in a double-well potential as an open quantum system. *Phys. Rev. A* **1998**, *58*, R50–R53. [CrossRef]
27. Meier, F.; Zwerger, W. Josephson tunneling between weakly interacting Bose-Einstein condensates. *Phys. Rev. A* **2001**, *64*, 033610. [CrossRef]
28. Paraoanu, G.S.; Kohler, S.; Sols, F.; Leggett, A.J. The Josephson plasmon as a Bogoliubov quasiparticle. *J. Phys. B At. Mol. Opt. Phys.* **2001**, *34*, 4689–4696. [CrossRef]
29. Kohler, S.; Sols, F. Chemical potential standard for atomic Bose–Einstein condensates. *New J. Phys.* **2003**, *5*, 94. [CrossRef]
30. Sakellari, E.; Leadbeater, M.; Kylstra, N.J.; Adams, C.S. Josephson spectroscopy of a dilute Bose-Einstein condensate in a double-well potential. *Phys. Rev. A* **2002**, *66*, 033612. [CrossRef]
31. Sakellari, E.; Proukakis, N.P.; Leadbeater, M.; Adams, C.S. Josephson tunnelling of a phase-imprinted Bose–Einstein condensate in a time-dependent double-well potential. *New J. Phys.* **2004**, *6*, 42. [CrossRef]
32. Zou, P.; Dalfovo, F. Josephson oscillations and self-trapping of superfluid fermions in a double-well potential. *J. Low Temp. Phys.* **2014**, *177*, 240. [CrossRef]
33. Abad, M.; Guilleumas, M.; Mayol, R.; Piazza, F.; Jezek, D. M.; Smerzi, A. Phase slips and vortex dynamics in Josephson oscillations between Bose-Einstein condensates. *EPL* **2015**, *109*, 40005. [CrossRef]
34. Bidasyuk, Y.M.; Weyrauch, M.; Momme, M.; Prikhodko, O.O. Finite-temperature dynamics of a bosonic Josephson junction. *J. Phys. B* **2018**, *51*, 205301. [CrossRef]
35. Polo, J.; Ahufinger, V.; Hekking, F.W.J.; Minguzzi, A. Damping of Josephson Oscillations in Strongly Correlated One-Dimensional Atomic Gases. *Phys. Rev. Lett.* **2018**, *121*, 090404. [CrossRef] [PubMed]
36. Polo, J.; Dubessy, R.; Pedri, P.; Perrin, H.; Minguzzi, A. Oscillations and Decay of Superfluid Currents in a One-Dimensional Bose Gas on a Ring. *Phys. Rev. Lett.* **2019**, *123*, 195301. [CrossRef]
37. Xhani, K.; Neri, E.; Galantucci, L.; Scazza, F.; Burchianti, A.; Lee, K.L.; Barenghi, C.F.; Trombettoni, A.; Inguscio, M.; Zaccanti, M.; et al. Critical Transport and Vortex Dynamics in a Thin Atomic Josephson Junction. *Phys. Rev. Lett.* **2020**, *124*, 045301. [CrossRef]
38. Xhani, K.; Galantucci, L.; Barenghi, C.F.; Roati, G.; Trombettoni, A.; Proukakis, N.P. Dynamical phase diagram of ultracold Josephson junctions. *New J. Phys.* **2020**, *22*, 123006. [CrossRef]
39. Xhani, K.; Proukakis, N.P. Dissipation in a finite-temperature atomic Josephson junction. *Phys. Rev. Res.* **2022**, *4*, 033205. [CrossRef]
40. Wlazłowski, G.; Xhani, K.; Tylutki, M.; Proukakis, N.P.; Magierski, P. Dissipation Mechanisms in Fermionic Josephson Junction. *Phys. Rev. Lett.* **2023**, *130*, 023003. [CrossRef]
41. Furutani, K.; Tempere, J.; Salasnich, L. Quantum effective action for the bosonic Josephson junction. *Phys. Rev. B* **2022**, *105*, 134510. [CrossRef]
42. Bardin, A.; Lorenzi, F.; Salasnich, L. Quantum fluctuations in atomic Josephson junctions: The role of dimensionality. *New J. Phys.* **2024**, *26*, 013021. [CrossRef]
43. Ji, S.C.; Schweigler, T.; Tajik, M.; Cataldini, F.; Sabino, J.a.; Møller, F.S.; Erne, S.; Schmiedmayer, J. Floquet Engineering a Bosonic Josephson Junction. *Phys. Rev. Lett.* **2022**, *129*, 080402. [CrossRef]

44. Pace, G.D.; Hernández-Rajkov, D.; Singh, V.P.; Grani, N.; Fernández, M.F.; Nesti, G.; Seman, J.A.; Inguscio, M.; Amico, L.; Roati, G. Shapiro steps in strongly-interacting Fermi gases. *arXiv* **2024**, arXiv:2409.03448. [CrossRef]
45. Bernhart, E.; Röhrle, M.; Singh, V.P.; Mathey, L.; Amico, L.; Ott, H. Observation of Shapiro steps in an ultracold atomic Josephson junction. *arXiv* **2024**, arXiv:2409.03340. [CrossRef]
46. Singh, V.P.; Luick, N.; Sobirey, L.; Mathey, L. Josephson junction dynamics in a two-dimensional ultracold Bose gas. *Phys. Rev. Res.* **2020**, *2*, 033298. [CrossRef]
47. Zaccanti, M.; Zwerger, W. Critical Josephson current in BCS-BEC–crossover superfluids. *Phys. Rev. A* **2019**, *100*, 063601. [CrossRef]
48. Piselli, V.; Pisani, L.; Strinati, G.C. Josephson current flowing through a nontrivial geometry: Role of pairing fluctuations across the BCS-BEC crossover. *Phys. Rev. B* **2023**, *108*, 214504. [CrossRef]
49. Gauthier, G.; Szigeti, S.S.; Reeves, M.T.; Baker, M.; Bell, T.A.; Rubinsztein-Dunlop, H.; Davis, M.J.; Neely, T.W. An atomtronic oscillator circuit for quantum gases. *arXiv* **2019**, arXiv:1903.04086.
50. Pigneur, M.; Berrada, T.; Bonneau, M.; Schumm, T.; Demler, E.; Schmiedmayer, J. Relaxation to a Phase-Locked Equilibrium State in a One-Dimensional Bosonic Josephson Junction. *Phys. Rev. Lett.* **2018**, *120*, 173601. [CrossRef]
51. Furutani, K.; Salasnich, L. Interaction-induced dissipative quantum phase transition in a head-to-tail atomic Josephson junction. *Phys. Rev. B* **2024**, *110*, L140503. [CrossRef]
52. Saha, A.K.; Dubessy, R. Dynamical phase diagram of a one-dimensional Bose gas in a box with a tunable weak link: From Bose-Josephson oscillations to shock waves. *Phys. Rev. A* **2021**, *104*, 023316. [CrossRef]
53. Momme, M.R.; Bidasyuk, Y.M.; Weyrauch, M. Collective excitations and tunneling dynamics in long bosonic Josephson junctions. *Phys. Rev. A* **2019**, *100*, 033601. [CrossRef]
54. Labouvie, R.; Santra, B.; Heun, S.; Wimberger, S.; Ott, H. Negative Differential Conductivity in an Interacting Quantum Gas. *Phys. Rev. Lett.* **2015**, *115*, 050601. [CrossRef]
55. Begg, S.E.; Davis, M.J.; Reeves, M.T. Nonequilibrium Transport in a Superfluid Josephson Junction Chain: Is There Negative Differential Conductivity? *Phys. Rev. Lett.* **2024**, *132*, 103402. [CrossRef] [PubMed]
56. Saha, A.K.; Ray, D.S.; Deb, B. Phase diffusion and fluctuations in a dissipative Bose-Josephson junction. *Phys. Rev. E* **2023**, *107*, 034141. [CrossRef] [PubMed]
57. Lagoudakis, K.G.; Pietka, B.; Wouters, M.; André, R.; Deveaud-Plédran, B. Coherent Oscillations in an Exciton-Polariton Josephson Junction. *Phys. Rev. Lett.* **2010**, *105*, 120403. [CrossRef]
58. Adiyatullin, A.F.; Anderson, M.D.; Flayac, H.; Portella-Oberli, M.T.; Jabeen, F.; Ouellet-Plamondon, C.; Sallen, G.C.; Deveaud, B. Periodic squeezing in a polariton Josephson junction. *Nat. Commun.* **2017**, *8*, 1329. [CrossRef] [PubMed]
59. D'Errico, C.; Abbate, S.S.; Modugno, G. Quantum transport in ultracold atoms. *Philos. Trans. Royal Soc. A* **2017**, *375*, 20160425.
60. Wright, K.C.; Blakestad, R.B.; Lobb, C.J.; Phillips, W.D.; Campbell, G.K. Driving Phase Slips in a Superfluid Atom Circuit with a Rotating Weak Link. *Phys. Rev. Lett.* **2013**, *110*, 025302. [CrossRef]
61. Griffin, A.; Nikuni, T.; Zaremba, E. *Bose-Condensed Gases at Finite Temperatures*; Cambridge University Press: Cambridge, UK, 2009. [CrossRef]
62. Jackson, B.; Zaremba, E. Modeling Bose-Einstein condensed gases at finite temperatures with N-body simulations. *Phys. Rev. A* **2002**, *66*, 033606. [CrossRef]
63. Proukakis, N.P.; Jackson, B. Finite-temperature models of Bose–Einstein condensation. *J. Phys. B At. Mol. Opt. Phys.* **2008**, *41*, 203002. [CrossRef]
64. Lee, K.L.; Proukakis, N.P. Non-equilibrium atomic condensates and mixtures: Collective modes, condensate growth and thermalisation. *J. Phys. B At. Mol. Opt. Phys.* **2016**, *49*, 214003. [CrossRef]
65. Lee, K.L.; Jørgensen, N.B.; Liu, I.K.; Wacker, L.; Arlt, J.J.; Proukakis, N.P. Phase separation and dynamics of two-component Bose-Einstein condensates. *Phys. Rev. A* **2016**, *94*, 013602. [CrossRef]
66. Blakie, P.B.; Bradley, A.S.; Davis, M.J.; Ballagh, R.J.; Gardiner, C.W. Dynamics and statistical mechanics of ultra-cold Bose gases using c-field techniques. *Adv. Phys.* **2008**, *57*, 363–455. [CrossRef]
67. Proukakis, N.; Gardiner, S.; Davis, M.; Szymańska, M. (Eds.) *Quantum Gases: Finite Temperature and Non-Equilibrium Dynamics*; Imperial College Press: London, UK, 2013.
68. Rooney, S.J.; Allen, A.J.; Zülicke, U.; Proukakis, N.P.; Bradley, A.S. Reservoir interactions of a vortex in a trapped three-dimensional Bose-Einstein condensate. *Phys. Rev. A* **2016**, *93*, 063603. [CrossRef]
69. Proukakis, N.P.; Rigopoulos, G.; Soto, A. Self-Consistent Stochastic Finite-Temperature Modelling: Ultracold Bose Gases with Local (s-wave) and Long-Range (Dipolar) Interactions. *arXiv* **2024**, arXiv:2407.20178.
70. Jackson, B.; Proukakis, N.P.; Barenghi, C.F.; Zaremba, E. Finite-temperature vortex dynamics in Bose-Einstein condensates. *Phys. Rev. A* **2009**, *79*, 053615. [CrossRef]
71. Jackson, B.; Proukakis, N.P.; Barenghi, C.F. Dark-soliton dynamics in Bose-Einstein condensates at finite temperature. *Phys. Rev. A* **2007**, *75*, 051601. [CrossRef]

72. Allen, A.J.; Zaremba, E.; Barenghi, C.F.; Proukakis, N.P. Observable vortex properties in finite-temperature Bose gases. *Phys. Rev. A* **2013**, *87*, 013630. [CrossRef]
73. Allen, A.J.; Zuccher, S.; Caliari, M.; Proukakis, N.P.; Parker, N.G.; Barenghi, C.F. Vortex reconnections in atomic condensates at finite temperature. *Phys. Rev. A* **2014**, *90*, 013601. [CrossRef]
74. Arahata, E.; Nikuni, T. Propagation of first and second sound in a highly elongated trapped Bose-condensed gas at finite temperatures. *Phys. Rev. A* **2013**, *87*, 033610. [CrossRef]
75. Märkle, J.; Allen, A.J.; Federsel, P.; Jetter, B.; Günther, A.; Fortágh, J.; Proukakis, N.P.; Judd, T.E. Evaporative cooling of cold atoms at surfaces. *Phys. Rev. A* **2014**, *90*, 023614. [CrossRef]
76. Jackson, B.; Zaremba, E. Quadrupole Collective Modes in Trapped Finite-Temperature Bose-Einstein Condensates. *Phys. Rev. Lett.* **2002**, *88*, 180402. [CrossRef]
77. Jackson, B.; Zaremba, E. Finite-Temperature Simulations of the Scissors Mode in Bose-Einstein Condensed Gases. *Phys. Rev. Lett.* **2001**, *87*, 100404. [CrossRef]
78. Straatsma, C.J.E.; Colussi, V.E.; Davis, M.J.; Lobser, D.S.; Holland, M.J.; Anderson, D.Z.; Lewandowski, H.J.; Cornell, E.A. Collapse and revival of the monopole mode of a degenerate Bose gas in an isotropic harmonic trap. *Phys. Rev. A* **2016**, *94*, 043640. [CrossRef]